Supplemental Information
Chiral current-driven effect induced by curvature gradient

G. H. R. Bittencourt,[1,2] M. Castro,[3] A. S. Nunez,[4] D. Altbir,[5] S. Allende,[3] and V. L. Carvalho-Santos[1,*]

[1] *Universidade Federal de Viçosa, Departamento de Física, Avenida Peter Henry Rolfs s/n, 36570-000, Viçosa, MG, Brazil.*
[2] *Instituto Federal de Santa Catarina, R. Aloísio Stoffel, 89885-000, São Carlos, SC, Brasil*
[3] *Universidad de Santiago de Chile, Departamento de Física, Avda. Víctor Jara 3493, Estación Central, CEDENNA, Santiago, Chile*
[4] *Departamento de Física, FCFM, Universidad de Chile, CEDENNA, Santiago, Chile*
[5] *Universidad Diego Portales, Ejército 441, CEDENNA, Santiago, Chile*

TRANSVERSE DW ENERGY

For our calculations, we parametrize the magnetization distribution using a Frenet-Serret basis as follows,

$$\mathbf{m} = m_1\,\hat{\mathbf{e}}_1 + m_2\,\hat{\mathbf{e}}_2 + m_3\,\hat{\mathbf{e}}_3\,, \tag{1}$$

where $\hat{\mathbf{e}}_1$, $\hat{\mathbf{e}}_2$, and $\hat{\mathbf{e}}_3$ are unitary vectors representing the tangential, normal and binormal directions, respectively. To obtain the exchange energy, it is convenient to define the derivatives of the unitary vectors as

$$\begin{bmatrix}\hat{\mathbf{e}}_1'\\ \hat{\mathbf{e}}_2'\\ \hat{\mathbf{e}}_3'\end{bmatrix} = F_{\alpha\beta}\cdot\begin{bmatrix}\hat{\mathbf{e}}_1\\ \hat{\mathbf{e}}_2\\ \hat{\mathbf{e}}_3\end{bmatrix}, \tag{2}$$

where

$$F_{\alpha\beta} = \begin{bmatrix}0 & \kappa & 0\\ -\kappa & 0 & 0\\ 0 & 0 & 0\end{bmatrix}, \tag{3}$$

being κ the curvature of a torsionless nanowire (NW). Here, the prime represents the derivative with respect to the natural parameter, s.

The exchange energy can be obtained as $E_{\rm ex} = \mathcal{S}A\int \mathcal{E}_{\rm ex}\,ds$, whose energy density, written in the Frenet-Serret referential frame reads $\mathcal{E}_{\rm ex} = (m_\alpha \mathbf{e}_\alpha)'(m_\beta \mathbf{e}_\beta)'$. Here, we use the Einstein convention, where a sum is associated with repeated indices. Under this framework, we can write the energy density as

$$\mathcal{E}_{\rm ex} = \mathcal{E}_{\rm ex}^{(0)} + \mathcal{E}_{\rm ex}^{(\rm DM)} + \mathcal{E}_{\rm ex}^{(\rm A)}\,, \tag{4a}$$

where $\mathcal{E}_{\rm ex}^{(0)} = |\mathbf{m}'|^2$, relates to the standard exchange energy in the Cartesian basis and $\mathcal{E}_{\rm ex}^{(\rm DM)} = F_{\alpha\beta}\left(m_\alpha m_\beta' - m_\alpha' m_\beta\right)$ and $\mathcal{E}_{\rm ex}^{(\rm A)} = \mathcal{K}_{\alpha\beta}m_\alpha m_\beta$ are the exchange-driven curvature-induced Dzyaloshinskii-Moriya and anisotropy, respectively. Here,

$$\mathcal{K}_{\alpha\beta} = F_{\alpha\gamma}F_{\beta\gamma} = \begin{bmatrix}\kappa^2 & 0 & 0\\ 0 & \kappa^2 & 0\\ 0 & 0 & 0\end{bmatrix}. \tag{5}$$

Now, we describe the magnetization components in a spherical coordinate system lying in the curvilinear basis as $\mathbf{m} = \cos\Omega\,\hat{\mathbf{e}}_1 + \sin\Omega\cos\Phi\,\hat{\mathbf{e}}_2 + \sin\Omega\sin\Phi\,\hat{\mathbf{e}}_3$. Then, the exchange energy density is evaluated as

$$\mathcal{E}_{\rm ex} = \mathcal{A}^2 + \mathcal{B}^2\,, \tag{6}$$

where $\mathcal{A} = \Omega' + \kappa\cos\Phi$ and $\mathcal{B} = \Phi'\sin\Omega - \kappa\cos\Omega\sin\Phi$.

As explained in the main text, the dipolar interaction can be obtained from the shape anisotropy approximation and can be written as

$$\mathcal{E}_{\rm d} = \frac{\mu_0}{2}M_s^2\sin^2\Omega\left(N_2\cos^2\Phi + N_3\sin^2\Phi\right), \tag{7}$$

where N_α is the demagnetizing factor related to the α-direction.

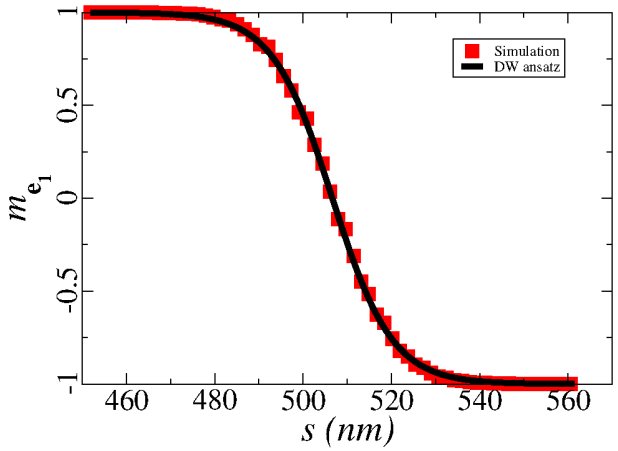

Figure 1. DW profile obtained by the adopted ansatz (black line) and micromagnetic simulations (red squares) for a NW with curvature $\kappa_0 = 5\pi\times10^{-3}$ nm^{-1}.

* vagson.santos@ufv.br

Now, we have represented the DW profile by the ansatz

$$\Omega(s) = 2\arctan\left[e^{\frac{p(s-q)}{\lambda}}\right], \tag{8}$$

where $p = \pm 1$, q is the DW center position, and λ is the DW width parameter. Finally, by assuming $\Phi = \phi$, with $\phi' = 0$, and integrating along the NW length, we obtain the exchange and dipolar energies given by Eqs. 4a and 4b in the main manuscript. We highlight that the DW profile obtained from the adopted ansatz agrees very well with micromagnetic simulations, as shown in Fig. 1.

CHIRAL TERM OF THE SPIN TRANSFER TORQUE ON THE TRANSVERSE DW

We start with the LLG equation to describe the magnetization, given by Eq. (1) in the main manuscript and presented here for clarity

$$\dot{\mathbf{m}} = \frac{\gamma}{M_s}\mathbf{m}\times\frac{\delta E}{\delta \mathbf{m}} + \alpha\,\mathbf{m}\times\dot{\mathbf{m}} + \boldsymbol{\Gamma}_u\,, \tag{9}$$

where

$$\boldsymbol{\Gamma}_u = \mathbf{m}\times[\mathbf{m}\times(\mathbf{u}\cdot\boldsymbol{\nabla})\,\mathbf{m}] + \beta\,\mathbf{m}\times(\mathbf{u}\cdot\boldsymbol{\nabla})\,\mathbf{m}\,. \tag{10}$$

By assuming $\mathbf{u} = u\,\hat{\mathbf{e}}_1$, we have that $(\mathbf{u}\cdot\boldsymbol{\nabla})\mathbf{m} = u\,\mathbf{m}'(s)$. For the adopted parametrization, we obtain

$$\boldsymbol{\Gamma}_u = -u\,(\mathcal{A}+\beta\,\mathcal{B})\,\hat{\Omega} + u\,(\beta\,\mathcal{A}-\mathcal{B})\,\hat{\Phi}\,, \tag{11}$$

where $\mathcal{A}$ and $\mathcal{B}$ are given in Eq. (6). Therefore, using the inner space basis (Ω, Φ), we can rewrite (9) as

$$-\sin\Omega\,(\dot{\Omega} + u\,\Omega') = \frac{\gamma}{M_s}\frac{\delta E}{\delta\Phi} + \alpha\,\dot{\Phi}\sin^2\Omega + u\,\kappa\,\sin\Omega\cos\Phi + u\,\beta\,\mathcal{B}\sin\Omega\,, \tag{12a}$$

$$\sin\Omega\,(\dot{\Phi} + u\Phi') = \frac{\gamma}{M_s}\frac{\delta E}{\delta\Omega} + \alpha\,\dot{\Omega} + u\,\beta\,\mathcal{A} + u\,\kappa\,\cos\Omega\sin\Phi\,. \tag{12b}$$

This pair of equations can also be obtained by solving the Euler-Lagrange formalism given by Eqs. (2) and (3) in the main manuscript.

Finally, to clarify the origin of the CSTT, it is instructive to write $\boldsymbol{\Gamma}_u = -\gamma\,\mathbf{m}\times(\mu_0\mathbf{H}_u)$, where $\mathbf{H}_u$ is the effective-like field associated with the spin-transfer torque. To analyze the DW motion, we focus on the component of $\mathbf{H}_u$ tangent to the NW axis, given by

$$\mathbf{H}_u\cdot\hat{\mathbf{e}}_1 = \frac{u}{\mu_0\gamma}\Big[\beta\sin\Omega\,(\Omega' + \kappa\cos\Phi) - \Phi'\sin^2\Omega + \frac{\kappa}{2}\sin 2\Omega\sin\Phi\Big]\,. \tag{13}$$

The third term in this expression corresponds to a curvature-dependent term that does not vanish for $\Phi = \pm\pi/2$, and has been presented in Eq. 7 in the main text.

To complete our description of the dynamical DW behavior, Fig. 2 shows $\sin\phi$ as a function of t for distinct DW initial orientations. It is worth noticing that the correspondent position (q as a function of t) is depicted in Fig. 3 of the main text. Fig. 2 evidences that the DW oscillations represent small deviations around $\phi \approx \pm\pi/2$. Therefore, since the DW does not perform a complete rotation around the NW axis, the dynamical regime observed occurs below the Walker limit.

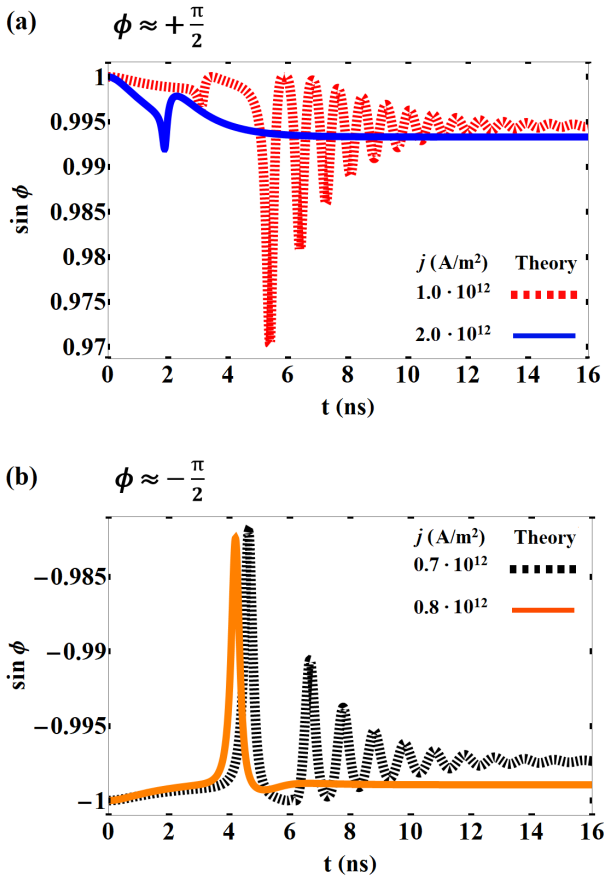

Figure 2. $\sin\phi$ as a function of time for different electric current values. Panels (a) and (b) show the results of a DW initially pointing along the $+\hat{\mathbf{z}}$ and $-\hat{\mathbf{z}}$ direction, respectively. In both cases, $\phi(t) \approx \pm\pi/2 + \delta\phi(t)$, being $\delta\phi(t)$ a decaying oscillatory contribution with small amplitude.

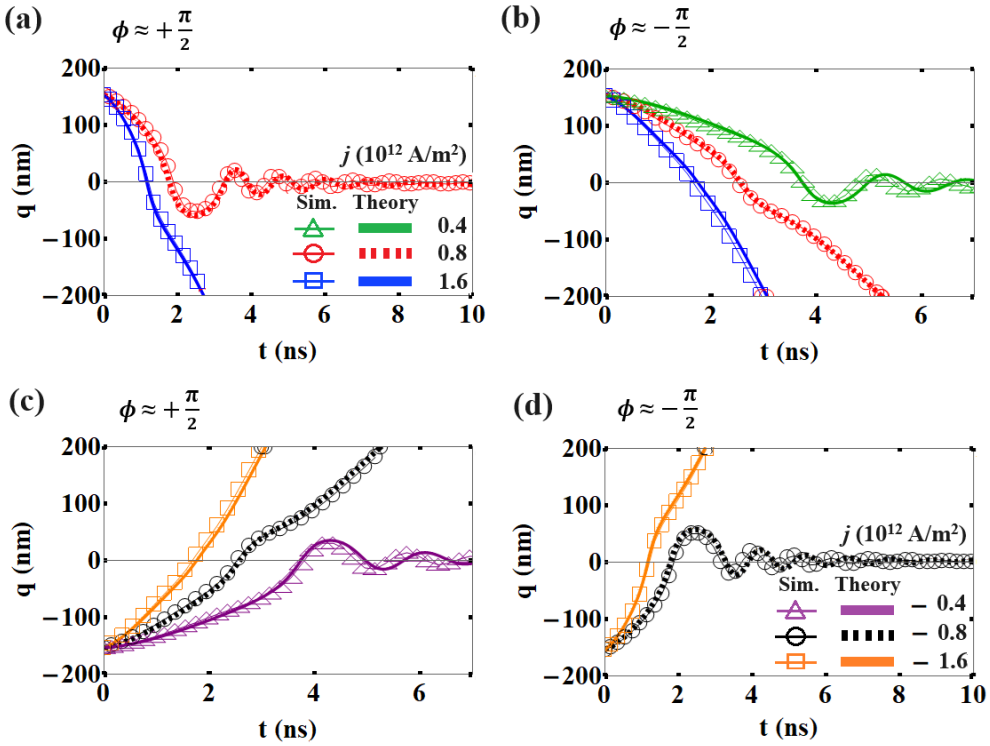

Figure 3. DW position as a function of time for different values of electric current for a NW with curvature $\kappa_0 = 5\pi \times 10^{-3}$ nm^{-1}. (a) and (c) show the results for DW pointing along the $+\hat{\boldsymbol{z}}$ direction, while (b) and (d) show the position when the DW center points along the $-\hat{\boldsymbol{z}}$ direction, respectively. Orange, black, purple, green, red, and blue lines show the results for $j = -1.6 \times 10^{12}$ A/m^2, $j = -0.8 \times 10^{12}$ A/m^2, $j = -0.4 \times 10^{12}$ A/m^2, $j = 0.4 \times 10^{12}$ A/m^2, $j = 0.8 \times 10^{12}$ A/m^2, and $j = 1.6 \times 10^{12}$ A/m^2, respectively.

RESULTS FOR OTHER VALUES OF NW CURVATURE

We have also obtained the transverse DW propagation for hyperbolic NWs with $\kappa_0 = 5\pi \times 10^{-3}$ nm^{-1}. Fig. (3) presents the obtained results for the DW position as a function of time for four different values of current density. Lines represent the analytical results, and symbols depict the DW position obtained from micromagnetic simulations. One notices that, for positive values of electric current, the CSTT is responsible for the DW pinning for $j = 0.8 \times 10^{12}$ A/m^2 when $\phi = +\pi/2$, while the DW crosses the region with maximum curvature when $\phi = -\pi/2$. By replacing the electric current direction, we observe the inverse behavior, where the CSTT is responsible for the DW pinning for $j = -0.8 \times 10^{12}$ A/m^2 when $\phi = -\pi/2$, and crosses the NW when $\phi = +\pi/2$.

Additionally, the analysis of the results for $\kappa_0 = 5\pi \times 10^{-3}$ nm^{-1} and $\kappa_0 = 6\pi \times 10^{-3}$ nm^{-1} (presented in the main manuscript), allows to conclude that the threshold values of the electric current for which the DW crosses the curved region decrease with the NW curvature. The smaller the κ_0, the smaller the j value for DW pinning. Finally, there are current values in which the DW can be pinned or cross the region with maximum curvature independent of its phase. As examples of this behavior, we show the DW position as a function of time for $|j| = 0.4 \times 10^{12}$ A/m^2 and $|j| = 1.6 \times 10^{12}$ A/m^2, respectively.